Available online at www.sciencedirect.com
ScienceDirect
Journal of Power Sources 163 (2007) 830–845
JOURNAL OF POWER SOURCES
www.elsevier.com/locate/jpowsour

Control relevant modeling of planer solid oxide fuel cell system

AKM M. Murshed, Biao Huang*, K. Nandakumar

Department of Chemical and Materials Engineering, University of Alberta, Edmonton, Alta. T6G 2G6, Canada

Received 18 July 2006; received in revised form 27 September 2006; accepted 29 September 2006
Available online 13 November 2006

Abstract

This paper provides two types of control relevant models of planer solid oxide fuel cell system with different details. Dynamic models of system components which include heat exchanger, reformer and after-burner are also provided along with the necessary formulation of a fuel cell connected in parallel with a capacitor. Steady-state and dynamic simulations of fuel cell system for both types of models are performed. The results indicate that both models are comparable in predicting stack voltage at lower current load. But, the discrepancy in the stack voltage, power and temperature of different components become more prominent at higher current load.

Keywords: Solid oxide; Fuel cell; SOFC; ODE; First principle model; BOP

1. Introduction

Fuel cells are electrochemical devices that generate electrical energy directly from chemical reactions. Unlike heat engine or gas turbine where there are losses due to Carnot cycle efficiency limitation and mechanical losses, chemical energy is directly converted to electrical energy and thus the fuel cell plant efficiency can be as high as 40–55%. In addition, the heat generation from the electrochemical reactions in a fuel cell can also be used for cogeneration applications increasing the efficiency up to 70%. Some other potential features of fuel cell include no moving parts, quiet operation, flexibility in fuel types and size of the fuel cell, and most of all rapid load following capability [23]. Another attractive feature of fuel cell is that it demonstrates same efficiency irrespective of its size, which makes it useful for a versatile range of applications including power generation for home or a commercial building, mobile equipments and automobile.

A large amount of work has been conducted on the modeling of solid oxide fuel cell from the viewpoint of fuel cell design, operability and performance, material selection and controller design [11,15,24,18,22,8]. The models can also be developed to simulate steady-state or dynamic behavior and can range from zero to three-dimensional [3,4]. For example, Padulles et al. [19] developed a simple model of a fuel cell-based power plant which included species dynamics but no temperature dynamics whereas, Hall and Colclaser [10] developed a more detailed model for simulating the transient operation of a tubular solid oxide fuel cell that included electrochemical, thermal and mass flow elements. The latter paper mainly focused on the effect of load change on the terminal voltage. The work presented in [1,5,15,4,2,12] investigated transient behavior of a planer SOFC due to load change using a multi-dimensional, time-dependent model and is useful for simulating fuel cell behavior. The models are expressed by a set of PDEs which are solved numerically to evaluate the performance of the fuel cell based on different design parameters. These models, since expressed as PDEs, are however not convenient for designing controllers. Sedghisigarchi and Feliachi [21] went a step further by considering chemical and thermal aspects of chemical reactions and ohmic, activation and concentration losses in the fuel cell stack. The authors however only considered lumped thermal models which is a drawback particularly for a hybrid fuel cell system in conjugation with combustor, turbine and heat exchangers for generating electricity where different flow streams have different temperature distributions. Several authors also developed models of fuel cell system for analyzing fuel cell performance [7,6,17,13]. Table 2.1 of [5] summarizes the chronological progression of planar SOFC modeling in terms of the underlying objectives.

In this paper, two sets of dynamic models of different details are presented by considering electro-chemical and thermal aspects of fuel cell. Both of the models are represented by a set of first-order ordinary differential equations and thus are useful

* Corresponding author. Tel.: +1 780 492 9016; fax: +1 780 492 2881.
E-mail address: biao.huang@ualberta.ca (B. Huang).

0378-7753/$ – see front matter © 2006 Elsevier B.V. All rights reserved.
doi:10.1016/j.jpowsour.2006.09.080

for simulating transient behavior of the fuel cell as well as designing model-based controllers. In addition, simplified thermal dynamic models of fuel cell system components are developed and connected to fuel cell to simulate the dynamic behavior of fuel cell system. The fuel cell system dynamic model consists of only nonlinear ordinary differential equation and thus can be utilized to design system-wide controller such as nonlinear MPC. The model can also be used to estimate unmeasured states using state estimators. In addition, the advantage of using capacitor connected in parallel with the fuel cell along with its formulation is also described.

The paper is organized as follows: first, general principle of the fuel cell is described followed by the modeling objective in Section 3; next, two sets of models, lumped and detail model, are presented in Section 4 and 5 followed by fuel cell simulation in Section 8.1. In this section, both dynamic and steady-state results are simulated and analyzed. Next the advantage of using a capacitor as an auxiliary power source is described along with necessary formulations in Section 6. In Sections 7 and 8.3, the fuel cell system model is developed and simulated to analyze performance of transient system.

2. General principle

A typical fuel cell consists of an electrolyte in contact with anode and cathode on either side. Hydrogen rich fuel and air are continuously fed into the fuel cell for generating electricity. The electrolyte acts as a barrier between anode and cathode allowing only certain types of ions to pass through it. Fuel cells are mainly classified depending on the nature of the electrolytes. Some of the most common fuel cells are molten carbonate fuel cell (MCFC), proton exchange membrane fuel cell (PEMFC), polymer electrolyte fuel cell (PEFC) and solid oxide fuel cell (SOFC) [23]. Solid oxide fuel cell, as its name suggests, uses a solid metal oxide as electrolyte. The cell operates at high temperature which makes it particularly useful for internal reforming of natural gases. The high temperature exit gases can be used further to generate electricity by a turbine. SOFC can be designed in different shapes and sizes due to the solid nature of the electrolyte, for example, planer and tubular. The high temperature of the SOFC however imposes a stringent requirements on the material selection due to the thermal expansion mismatch between anode, electrolyte, cathode and connector materials. Thus, it is important to operate SOFC in such a way that the stack temperature remains within the design range.

In a planer SOFC, several cells are stacked and connected in series to complete the circuit. At each cell, hydrogen releases electrons at the anode surface which travel through the outer circuit and combine with oxygen to produce oxide ions. Electrolyte which acts as a separator between hydrogen and oxygen, and thus prevents direct combustion, allows only certain types of positive ions to pass through it. SOFC usually uses Y_2O_3-stabilized ZO_2 (YSZ) as electrolyte which allows oxide ion to pass through it to reach the anode surface, where the oxide ion combines with H^+ to form water. The reactions can be summarized as follows:

$$\text{Anode:} \quad H_2 \rightarrow 2H^+ + 2e \tag{1}$$

$$\text{Cathode:} \quad \tfrac{1}{2}O_2 + 2e \rightarrow O^{2-} \tag{2}$$

$$\text{Overall:} \quad H_2 + \tfrac{1}{2}O_2 \rightarrow H_2O + \text{heat} \tag{3}$$

The electrode potential difference, ΔE that drives the reaction to take place and flow of ions through the circuit can be expressed by Nernst equation:

$$\Delta E = \Delta E_0 + \frac{RT}{2F} \ln \frac{p_{H_2} p_{O_2}^{0.5}}{p_{H_2O}} \tag{4}$$

where ΔE_0 [V] is the standard cell potential; p_{H_2}, p_{O_2} and p_{H_2O} the partial pressures of hydrogen, oxygen and steam [atm]; T [K] the cell electrode temperature at which the reaction is taking place; and R [=1 atm kmol^{-1} K^{-1}] and F [=96485.34 s A/mol] are the universal gas constant and the Faraday's constant, respectively. The Nernst model in Eq. (4) can thus be used to predict cell voltage provided standard cell potential, partial pressures and electrode temperature are known which can be derived in terms of species and energy balances.

3. Modeling objective

Knowledge of the transient and steady-state response of the solid oxide fuel cell is important for studying fuel cell performance as well as designing the controller. The level of modeling sophistication thus depends on the objective and can vary from simple linear state–space models to complex 3-D models. The models can also specifically be derived to simulate steady-state or dynamic behavior.

Since in this work, the modeling objective is driven by the requirement of a control relevant dynamic model that can predict the cell terminal voltage and system component temperatures as well as design controller with relative ease, certain model characteristics have to be identified:

- The model should comprise a set of linear or, nonlinear ODEs to predict transient behavior of the fuel cell. In other words the model should be zero-dimensional to avoid distributed model comprising of a set of PDEs which makes it difficult to design controllers.
- It should be able to predict all the important variables including terminal voltage, pressure and temperature.
- Model should be valid for all operating regions, which is the main driving factor for building a first principle model rather than a data-based model.

Based on these modeling objectives, two types of models are presented in the following sections. First, a completely "lumped model" is derived which assumes uniform temperature throughout the cell including both the solid phase and the gas phase. Even though this assumption is fairly valid at lower current load, where the temperatures of electrode, interconnector and unreacted gases do not differ much, at higher current load, this may not be the case. Thus, a second model, named, "detail model"

is presented which assumes that different components namely electrode, interconnector, fuel and air have different temperature distributions. Note that the term "detail model" used in this paper is relative to the completely lumped model. In addition, lumped thermal models for the balance of fuel cell system, e.g., heat exchangers, reformer and burner are presented and then integrated with lumped and detailed model, respectively, to simulate dynamic behavior of fuel cell system stack voltage due to load changes and other disturbances.

4. Lumped model

The lumped model of a stand-alone planer solid oxide fuel cell fed with hydrogen and air is developed based on the following assumptions:

- The gases are ideal.
- Pressure is constant inside the gas channel.
- The ratio of interior and exterior pressures is large enough to consider that the orifice is choked.
- Uniform temperature distribution for the entire fuel cell stack.
- Ideal mixing of gas inside the fuel cell stack. Hence, the exit temperature fuel and air are same as the inside temperature.
- Heat capacities of the fuel and air are negligible.
- Negligible heat loss to the surroundings.
- The Nernst equation can be applied for calculating voltage.

Based on these assumptions an overall material and energy balance is performed around the fuel cell stack as shown in Fig. 1(a).

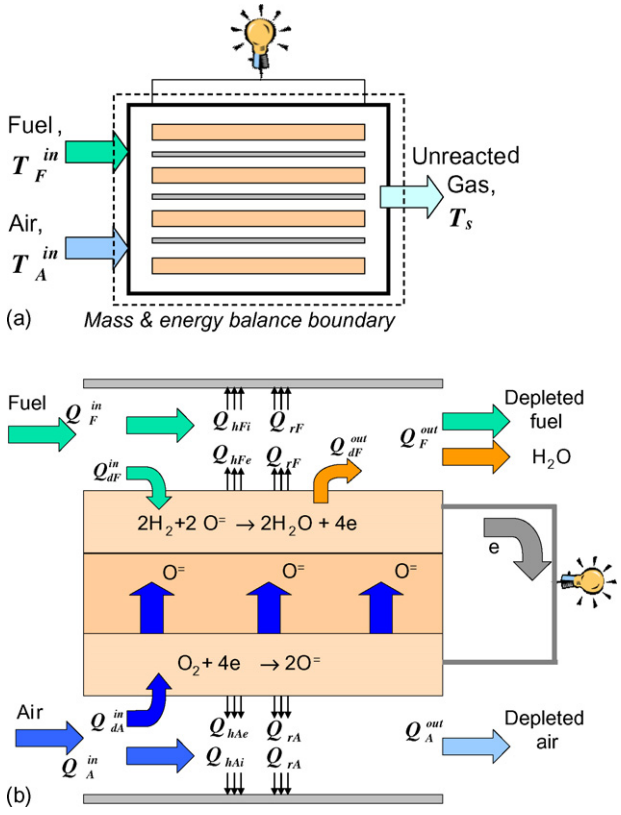

Fig. 1. Schematic diagram of: (a) the lumped model and (b) the detail model

4.1. Species balance

The ith component material balance for the fuel cell stack can be written as [9,21]:

$$\frac{PV}{RT_s}\frac{dx_i}{dt} = \dot{n}_i^{in} - \dot{n}_i^{out} + \dot{n}_i^{r} \tag{5}$$

where P [atm] and T_s [K] are the stack pressure and temperature; V [m^3] the compartment volume; x_i the exit molarity of the ith component; and $\dot{n}_i^{in}$, $\dot{n}_i^{out}$ and $\dot{n}_i^{r}$ are the inlet, outlet and reactive molar flow rates of the ith component in mol s^{-1}.

Component balance for hydrogen in terms of its partial pressure p_{H_2} can thus be expressed as:

$$\frac{dp_{H_2}}{dt} = \frac{RT_s}{V_{an}}(\dot{n}_{H_2}^{in} - \dot{n}_{H_2}^{out} - \dot{n}_{H_2}^{r}) \tag{6}$$

where V_{an} [m^3] is the anode compartment volume; and $\dot{n}_{H_2}^{in}$, $\dot{n}_{H_2}^{out}$ and $\dot{n}_{H_2}^{r}$ are the inlet, outlet and reactive molar flow rates of H_2 [mol s^{-1}]. The reactive and exit flow rates of hydrogen can be expressed by [19]:

$$\dot{n}_{H_2}^{r} = 2K_r I \tag{7}$$

$$\dot{n}_{H_2}^{out} = K_{H_2} p_{H_2} \tag{8}$$

where $K_r = N_0/4F$; I [A] the stack current; N_0 the number of cells associated in series in the stack; and K_{H_2} is the valve molar constant for hydrogen.

Defining $\tau_{H_2} = V_{an}/K_{H_2}RT_s$, Eq. (6) can then be written as:

$$\frac{d}{dt}p_{H_2} = \frac{1}{\tau_{H_2}K_{H_2}}(q_{H_2}^{in} - K_{H_2}p_{H_2} - 2K_r I) \tag{9}$$

Since K_{H_2} is a constant, τ_{H_2} is a function of cell temperature only and can be expressed as $\tau_{H_2} = \tau_{H_2}^* T^*/T_s$ where $\tau_{H_2}^* = \tau_{H_2}|_{T_s=T^*}$. Eq. (9) thus can be rewritten as:

$$\frac{dp_{H_2}}{dt} = \frac{T_s}{K_{H_2}\tau_{H_2}^* T^*}(\dot{n}_{H_2}^{in} - K_{H_2}p_{H_2} - 2K_r I) \tag{10}$$

Similarly component balances for O_2 and H_2O lead to the following set of equations:

$$\frac{dp_{O_2}}{dt} = \frac{T_s}{K_{O_2}\tau_{O_2}^* T^*}(q_{O_2}^{in} - K_{O_2}p_{O_2} - K_r I) \tag{11}$$

and,

$$\frac{dp_{H_2O}}{dt} = \frac{T_s}{K_{H_2O}\tau_{H_2O}^* T^*}(q_{H_2O}^{in} - K_{H_2O}p_{H_2O} + 2K_r I) \tag{12}$$

4.2. Energy balance

In the lumped stack modeling, it is assumed that there is no temperature variation inside the fuel cell which means that all the components of the fuel cell—electrode, interconnector and gases inside channels posses the same temperature at any instance. It is further assumed that the heat capacity of the gases inside the channels are negligible compared to the solid components of the fuel cell. Then the dynamic model of the cell temperature, T_s,

can be found by performing energy balance around the entire fuel cell stack:

$$m_s \bar{C}_{ps} \frac{dT_s}{dt} = \sum \dot{n}_i^{in} \int_{T_{ref}}^{T_{in}} C_{p,i}(T)\, dT - \sum \dot{n}_i^{out} \times \int_{T_{ref}}^{T_s} C_{p,i}(T)\, dT - \dot{n}_{H_2}^r \Delta \hat{H}_r^\circ - V_s I \quad (13)$$

where m_s and $\bar{C}_{ps}$ are the mass and average specific heat of fuel cell materials excluding gases; $C_{p,i}$ the specific heat of ith fuel or air gas entering the system; $\Delta \hat{H}_r^\circ$ the specific heat of reaction of Eq. (3); and V_s is the stack voltage.

4.3. Stack voltage

Applying Nernst's equation and considering ohmic, activation and concentration polarization, the stack voltage can be expressed as,

$$V_s = V_0 - \eta_{ohm} - \eta_{act} - \eta_{con} \quad (14)$$

where the open circuit voltage, V_0, is

$$V_0 = N_0 \Delta E = N_0 \left[\Delta E_0 + \frac{RT_s}{2F} \ln \frac{p_{H_2} p_{O_2}^{0.5}}{p_{H_2O}} \right] \quad (15)$$

Here, standard cell potential ΔE_0 exhibits linear relationship with cell temperature and can be approximated from the experimental data provided in Table 2-3 of [23]:

$$\Delta E_0\,(V) = 1.2586 - 0.000252 T_s\,(K) \quad (16)$$

Ohmic polarization occurs because of resistance to the flow of ions through different components of cell materials. The loss can be expressed as:

$$\eta_{ohm} = r(T_s) I \quad (17)$$

The cell resistance, $r(T_s)$, however, is a function of cell electrode temperature and can be expressed by the second-order Steinhart Hart equation:

$$r(T_s) = r_0 \exp\left[\alpha \left(\frac{1}{T_s} - \frac{1}{T_0} \right)\right] \quad (18)$$

where r_0 [Ω] is the internal resistance at temperature T_0 [K] and α is a constant.

Activation and concentration polarization can be calculated by the following equations [5,21,14]:

$$\eta_{act} = a + b \log I \quad (19)$$

and,

$$\eta_{con} = \frac{RT_s}{2F} \ln\left(1 - \frac{I}{I_L}\right) \quad (20)$$

where a and b are the Tafel constant and Tafel slope, respectively; and I_L is the limiting current.

5. Detail model

As stated earlier, at higher current load the assumption of uniform temperature distribution throughout the fuel cell in lumped model, as described in Section 4, may not be valid. Thus, in this section a relatively more detail model is developed where it is assumed that different cell components have different temperature distributions and thus the model is "detailed" compared to the "lumped" model. The major assumptions that differentiate it from the lumped model are described below:

- Different temperatures among electrode, interconnector, fuel and air side gases.
- Ideal mixing of gases inside the fuel cell channels so that fuel and air exit temperatures are same as the temperature inside the fuel and air channels, respectively.
- No temperature variation in the axial direction.

Based on these assumptions material and energy balances are performed around electrode, interconnector, fuel gas channel and air gas channel of the fuel cell as depicted in Fig. 1(b). Since in this model only temperature distributions are assumed to be different, species balance around the cell remains same as described in Section 4.1, and so is the cell voltage calculation in Section 4.3. The stack temperature T_s in Eqs. (15), (16), (18) and (20) however has to be replaced by electrode temperature, T_e.

5.1. Energy balance around electrode

The electrode control volume consists of the anode, electrolyte and the cathode. Even though the electro-chemical reactions take place at the anode and cathode near the surfaces of the electrolyte, and thus have temperature variations in the direction vertical to the surface area, it can be assumed constant due to very small thickness of the electrode. The temperature variation along the flow direction is also assumed constant, and thus the electrode temperature T_e dynamics can be expressed as a function of diffusive, convective, radiative and reactive heat transfer terms (Fig. 1(b)):

$$\rho_e A_c \Delta w_e \bar{C}_{pe} \frac{dT_e}{dt} = (Q_{dF}^{in} - Q_{dF}^{out}) + (Q_{dA}^{in} - Q_{dA}^{out}) - (Q_{hFe} + Q_{rF} + Q_{hAe} + Q_{rA}) - Q^r - \dot{W} \quad (21)$$

Here, A_c, Δw_e, ρ_e and $\bar{C}_{pe}$ are the electro-chemical surface area, thickness, density and specific heat of the electrode material, respectively. The fuel side diffusion heat terms in Eq. (21) can be expressed as:

$$Q_{dF}^{in} = \dot{n}_{H_2}^r \int_{T_{ref}}^{T_F} C_{p,H_2}(T)\, dT \quad (22)$$

$$Q_{dF}^{out} = \dot{n}_{H_2O}^r \int_{T_{ref}}^{T_F} C_{p,H_2O}(T)\, dT \quad (23)$$

where $\dot{n}_{H_2}^r = \dot{n}_{H_2O}^r = 2K_r I$, and T_F is the exit temperature of the depleted fuel. The air side heat transfer terms in and out of the electrode through diffusion in Eq. (21) can be expressed as:

$$Q_{dA}^{in} = \dot{n}_{O_2}^r \int_{T_{ref}}^{T_A} C_{p,O_2}(T)\, dT \quad (24)$$

$$Q_{\mathrm{dA}}^{\mathrm{out}} = 0 \tag{25}$$

where $\dot{n}_{\mathrm{O}_2}^{\mathrm{r}} = K_{\mathrm{r}} I$, and T_{A} is the exit temperature of depleted air. The convective heat transfers between electrode and fuel/air gases in Eq. (21) can be written as:

$$Q_{\mathrm{hFe}} = h_{\mathrm{Fe}} A_{\mathrm{c}} (T_{\mathrm{e}} - T_{\mathrm{F}}) \tag{26}$$

$$Q_{\mathrm{hAe}} = h_{\mathrm{Ae}} A_{\mathrm{c}} (T_{\mathrm{e}} - T_{\mathrm{A}}) \tag{27}$$

Here, the fuel side and air side heat transfer coefficients h_{Fe} and h_{Ae} are also functions of T_{F} and T_{A}, respectively, and are evaluated at each instance empirically [16,20]. The radiative heat transfer terms between electrode and interconnector of fuel side and air side in Eq. (21) can be expressed as:

$$Q_{\mathrm{rF}} = \frac{\sigma A_{\mathrm{c}} (T_{\mathrm{e}}^4 - T_{\mathrm{i}}^4)}{(1/\epsilon_{\mathrm{a}}) + (1/\epsilon_{\mathrm{i}}) - 1} \tag{28}$$

$$Q_{\mathrm{rA}} = \frac{\sigma A_{\mathrm{c}} (T_{\mathrm{e}}^4 - T_{\mathrm{i}}^4)}{(1/\epsilon_{\mathrm{c}}) + (1/\epsilon_{\mathrm{i}}) - 1} \tag{29}$$

where $\sigma = 5.6704 \times 10^{-8}\,\mathrm{W\,m^{-2}\,K^{-4}}$ is the Boltzman constant; T_{i} [K] the interconnector temperature; and ϵ_{a}, ϵ_{c} and ϵ_{i} are the emmisivity constants of anode, cathode and interconnector materials, respectively. The geometric factor of radiation in this case is assumed to be 1. Last, the heat generation and shaft work done by the fuel cell can be expressed as:

$$Q^{\mathrm{r}} = -\dot{n}_{\mathrm{H}_2}^{\mathrm{r}} \Delta \hat{H}_{\mathrm{r}}^{\circ} \quad \text{and} \quad \dot{W} = V_{\mathrm{s}} I \tag{30}$$

5.2. Energy balance around interconnector

The interconnector temperature, T_{i} dynamics can be expressed by the following equation:

$$\rho_{\mathrm{i}} A_{\mathrm{i}}\, \Delta w_{\mathrm{i}} \bar{C}_{pi} \frac{\mathrm{d}T_{\mathrm{i}}}{\mathrm{d}t} = Q_{\mathrm{hFi}} + Q_{\mathrm{rF}} + Q_{\mathrm{hAi}} + Q_{\mathrm{rA}} \tag{31}$$

where ρ_{i}, A_{i}, Δw_{i}, $\bar{C}_{pi}$ and T_{i} are the density, area, thickness, specific heat and temperature of the interconnect materials, respectively. Convective heat transfers between interconnect and fuel/air in Eq. (31) can be expressed as:

$$Q_{\mathrm{hFi}} = h_{\mathrm{Fi}} A_{\mathrm{i}} (T_{\mathrm{F}}^{\mathrm{out}} - T_{\mathrm{i}}) \tag{32}$$

$$Q_{\mathrm{hAi}} = h_{\mathrm{Ai}} A_{\mathrm{i}} (T_{\mathrm{A}}^{\mathrm{out}} - T_{\mathrm{i}}) \tag{33}$$

where h_{Fi} and h_{Ai} are fuel side and air side convective heat transfer coefficients adjacent to the interconnector surface, respectively, which are estimated empirically at each instance. The radiative heat transfer terms in Eq. (31) are expressed in Eqs. (28) and (29). For planer SOFC the area A_{i} can be approximated as the electro-chemical surface area, A_{c}.

5.3. Energy balance around fuel side

The dynamic model of exit fuel temperature, T_{F} can be expressed as:

$$\sum \frac{p_{\mathrm{i}} V_{\mathrm{channel}} C_{pi}^{\mathrm{out}}}{R T_{\mathrm{F}}} \frac{\mathrm{d}T_{\mathrm{F}}}{\mathrm{d}t} = (Q_{\mathrm{F}}^{\mathrm{in}} - Q_{\mathrm{F}}^{\mathrm{out}}) + (Q_{\mathrm{dF}}^{\mathrm{out}} - Q_{\mathrm{dF}}^{\mathrm{in}}) + (Q_{\mathrm{hFe}} - Q_{\mathrm{hFi}}) \tag{34}$$

Here, heat in, $Q_{\mathrm{F}}^{\mathrm{in}}$, and heat out, $Q_{\mathrm{F}}^{\mathrm{out}}$, of fuel cell by fuel flow can be expressed as:

$$Q_{\mathrm{F}}^{\mathrm{in}} = \sum \dot{n}_i^{\mathrm{in}} \int_{T_{\mathrm{ref}}}^{T_{\mathrm{F}}^{\mathrm{in}}} C_{p,i}(T)\,\mathrm{d}T \tag{35}$$

$$Q_{\mathrm{F}}^{\mathrm{out}} = \sum \dot{n}_i^{\mathrm{out}} \int_{T_{\mathrm{ref}}}^{T_{\mathrm{F}}} C_{p,i}(T)\,\mathrm{d}T \tag{36}$$

where $T_{\mathrm{F}}^{\mathrm{in}}$ is the temperature of fuel entering the SOFC. The diffusive and convective heat transfer terms $Q_{\mathrm{dF}}^{\mathrm{in}}$, $Q_{\mathrm{dF}}^{\mathrm{out}}$, Q_{hFe} and Q_{hFi} in Eq. (34) are expressed in Eqs. (22), (23), (26) and (32), respectively. If the energy stored by fuel gas is assumed to be negligible and the specific heats of fuel gases are assumed to be constant over the operating temperature region, then Eq. (34) reduces to an algebraic equation:

$$T_{\mathrm{F}} = \frac{N_{\mathrm{F}}}{D_{\mathrm{F}}} \tag{37}$$

where

$$N_{\mathrm{F}} = -Q_{\mathrm{F}}^{\mathrm{in}} + \overbrace{-h_{\mathrm{Fe}} A_{\mathrm{c}} T_{\mathrm{e}} - h_{\mathrm{Fi}} A_{\mathrm{i}} T_{\mathrm{i}}}^{-h_{\mathrm{F}} A_{\mathrm{c}} (T_{\mathrm{e}} + T_{\mathrm{i}})} + \left[-\sum \dot{n}_i^{\mathrm{out}} \bar{C}_{p,i}^{\mathrm{out}} + \dot{n}_{\mathrm{H_2O}}^{\mathrm{r}} \bar{C}_{p,\mathrm{H_2O}}^{\mathrm{out}} - \dot{n}_{\mathrm{H_2}}^{\mathrm{r}} \bar{C}_{p,\mathrm{H_2}}^{\mathrm{out}} \right] T_{\mathrm{ref}}$$

$$D_{\mathrm{F}} = \dot{n}_{\mathrm{H_2O}}^{\mathrm{r}} \bar{C}_{p,\mathrm{H_2O}}^{\mathrm{out}} - \dot{n}_{\mathrm{H_2}}^{\mathrm{r}} \bar{C}_{p,\mathrm{H_2}}^{\mathrm{out}} - \sum \dot{n}_i^{\mathrm{out}} \bar{C}_{p,i}^{\mathrm{out}} \underbrace{-h_{\mathrm{Fe}} A_{\mathrm{c}} - h_{\mathrm{Fi}} A_{\mathrm{i}}}_{-2h_{\mathrm{F}} A_{\mathrm{c}}}$$

5.4. Energy balance around air side

The dynamic model of air exit temperature, T_{A} can be expressed as:

$$\sum \frac{p_{\mathrm{i}} V_{\mathrm{channel}} C_{pi}^{\mathrm{out}}}{R T_{\mathrm{A}}} \frac{\mathrm{d}T_{\mathrm{A}}}{\mathrm{d}t} = (Q_{\mathrm{A}}^{\mathrm{in}} - Q_{\mathrm{A}}^{\mathrm{out}}) + (Q_{\mathrm{dA}}^{\mathrm{out}} - Q_{\mathrm{dA}}^{\mathrm{in}}) + (Q_{\mathrm{hAe}} - Q_{\mathrm{hAi}}) \tag{38}$$

Here, $Q_{\mathrm{A}}^{\mathrm{in}}$ and $Q_{\mathrm{A}}^{\mathrm{out}}$ are heat in and out of fuel cell through air flow and can be expressed as:

$$Q_{\mathrm{A}}^{\mathrm{in}} = \sum \dot{n}_i^{\mathrm{in}} \int_{T_{\mathrm{ref}}}^{T_{\mathrm{A}}^{\mathrm{in}}} C_{p,i}(T)\,\mathrm{d}T \tag{39}$$

$$Q_{\mathrm{A}}^{\mathrm{out}} = \sum \dot{n}_i^{\mathrm{out}} \int_{T_{\mathrm{ref}}}^{T_{\mathrm{A}}} C_{p,i}(T)\,\mathrm{d}T \tag{40}$$

The diffusive and convective heat transfer terms $Q_{\mathrm{dA}}^{\mathrm{in}}$, $Q_{\mathrm{dA}}^{\mathrm{out}}$, Q_{hAe} and Q_{hAi} in Eq. (38) are expressed in Eqs. (24), (25), (27) and (33). Assuming energy stored by the air is negligible and constant specific heat of air gases for the operating temperature range, the dynamic equation of T_{A} can also be reduced to

an algebraic equation:

$$T_A = \frac{N_A}{D_A} \tag{41}$$

where

$$N_A = -Q_A^{in} - \left[\sum \dot{n}_i^{out} \bar{C}_{p,i}^{out} - \dot{n}_{O_2}^{r} \bar{C}_{p,O_2}^{out}\right] T_{ref} \overbrace{-h_{Ae} A_c T_e - h_{Ai} A_i T_i}^{-h_A A_c (T_e + T_i)}$$

$$D_A = -\sum \dot{n}_i^{out} \bar{C}_{p,i}^{out} - \dot{n}_{O_2}^{r} \bar{C}_{p,O_2}^{out} \underbrace{-h_{Ae} A_c - h_{Ai} A_i}_{-2h_A A_c}$$

6. SOFC along with capacitor

For a stand-alone solid oxide fuel cell, the model equations describing the fuel cell behavior are expressed by the species balance [Eqs. (10)–(12)], energy balance [Eqs. (13), (21), (31), (34) and (38)] and the stack voltage equation [Eq. (14)]. These equations can be put in a concise form by:

$$\dot{x} = f(x, \dot{n}_i, I_d, V_s) \tag{42}$$

$$V_s = V_0(x) - r(x) I_d \tag{43}$$

where x contains the states describing the partial pressures and temperatures of the SOFC models; $\dot{n}_i$ the inlet flow rates of fuel or air; I_d the demand current load which passes through the fuel cell; and V_s is the stack voltage produced by the fuel cell. For simplicity, only ohmic loss has been taken into consideration in the above output equation. For a stand-alone fuel cell, the fuel cell current I_{fc} equals the demand current I_d. From the output equation, it is evident that a sudden change in the demand current will be associated with an instantaneous change in the stack voltage as shown by the transient responses (Fig. 6). This instantaneous change in the stack voltage can not be avoided no matter what type of advanced control is used due to the constraints on the manipulated variables that are typically the inlet fuel and air flow rates. To avoid this sudden loss in voltage and possible damage to electrical equipment, an ultra-capacitor of sufficient capacity can be used in parallel with the fuel cell as an auxiliary power source as shown in Fig. 2. The advantage of the capacitor can be seen intuitively—when there is a sudden change in the demand current, the capacitor will share the load and provide additional power. Thus, instead of sudden drop in the stack voltage, it drops smoothly depending on the capacitance of the ultra-capacitor. This gives an added boost to the controller connected to the SOFC system to keep the voltage at its referenced value. By avoiding sudden drop of the voltage the controller copes with only the slow change of the voltage and can bring the voltage at its reference value by increasing fuel flow rates within its constraints more easily. Mathematically this can be expressed as follows.

Assume that the current through the capacitor and the fuel cell are I_{uc} and I_{fc}, respectively. Then I_{fc} can be expressed in terms of the demand current as,

$$I_{fc} = I_d - I_{uc} \tag{44}$$

From the definition of capacitance, the current passing through an ultra-capacitor connected in parallel with a dc voltage source

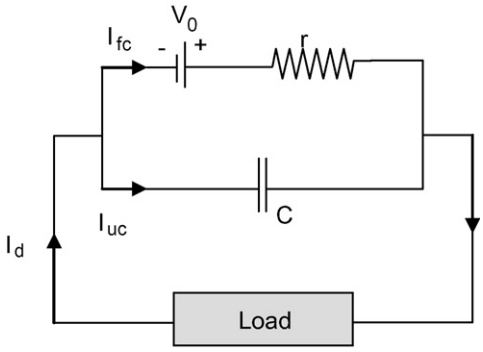

Fig. 2. Fuel cell along with a capacitor.

can be expressed as,

$$I_{uc} = -C \frac{dV_s}{dt} \tag{45}$$

where C is the capacitance [F] and V_s is the terminal voltage across the capacitor and the dc voltage source. Then current through the fuel cell can be rewritten as,

$$I_{fc} = I_d + C \frac{dV_s}{dt} \tag{46}$$

Stack voltage of the fuel cell as described by the output equation (43) then can be written as,

$$rC \frac{dV_s}{dt} = V_0 - rI_d - V_s \tag{47}$$

From Eq. (47), it is seen that the stack voltage has now taken the form of a first-order ODE instead of a static nonlinear output equation. Thus, instead of sudden voltage drop for a step increase in the demand current, the voltage drop slows down depending on the term rC, as shown in Section 8.2.

7. Fuel cell system

In the previous sections, a stand-alone fuel cell is described and modeled which can be used for simulating open loop transient behavior or designing model-based control. The SOFC under consideration is fed with H_2 as fuel and air as a source of O_2. But in practical situations a fuel cell is often associated with other components so that the SOFC plant can be fed with natural gas or other hydrogen rich fuel instead of pure hydrogen. One such SOFC system is shown in Fig. 3 which includes a reformer for converting methane (CH_4) into hydrogen, two heat exchangers for preheating fuel and air before feeding them into the reformer and fuel cell stack, respectively, one burner for burning unreacted fuel and, compressors for blowing fuel, air and steam. Often the fuel cell system includes a turbine to generate auxiliary power from the exhaust gas, fuel processing unit (e.g., desulphurizer) and a power conditioning unit (e.g., a voltage regulator, a dc/dc or dc/ac converter). These components are an integral part of the fuel cell system and called as *balance of plant* (BOP). Examples of process flow diagrams of SOFC systems are given in Fig. 1-14 of [23] and in Figs. 3.1, 3.2, 3.12 and 3.14 of [5].

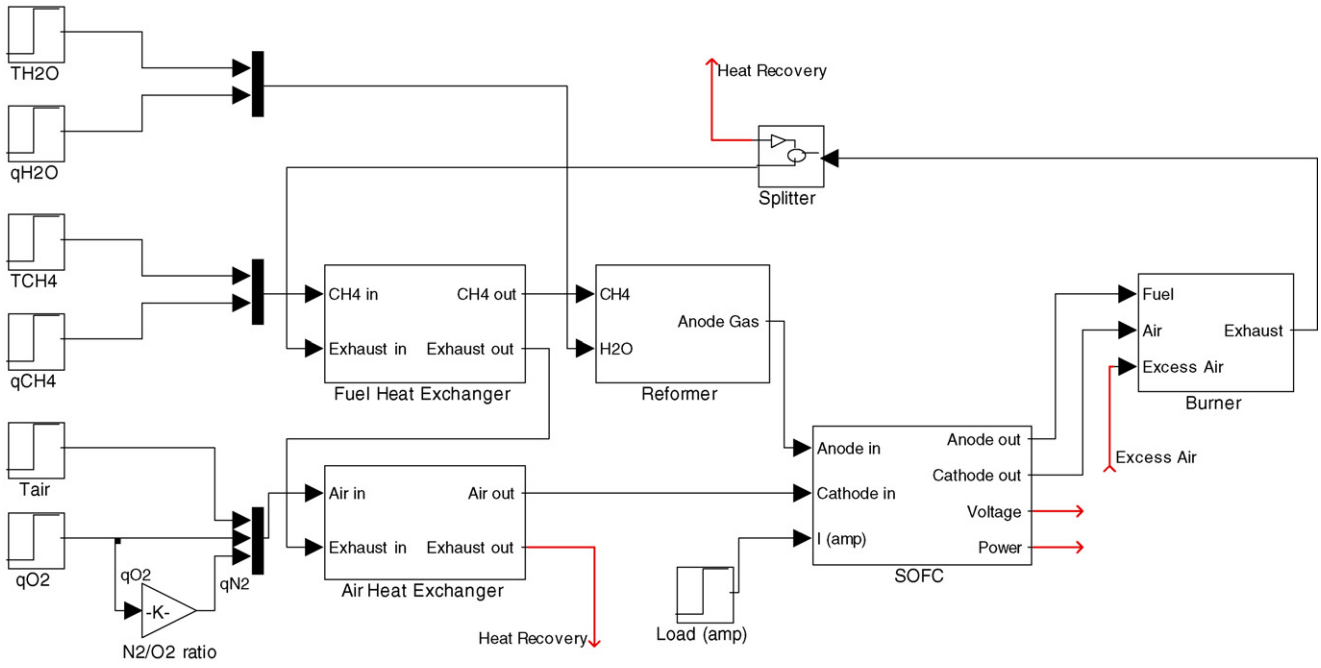

Fig. 3. SOFC system with heat exchangers, reformer, burner and splitter.

In the SOFC system that is simulated in this work (Fig. 3), methane is pressurized and fed to the fuel heat exchanger for preheating by the exhaust gas from the burner. The preheated methane then enters an external reformer along with steam where methane is being converted to hydrogen through reforming and water–gas shift reaction. The product gas from reformer enters into the anode compartment of the fuel cell stack. Pressurized air is also preheated in another heat exchanger by the hot exit gas from the fuel heat exchanger and sent to the cathode compartment of the fuel cell stack. Hydrogen from the anode compartment and oxygen from the cathode takes part into the electrochemical reactions to produce power at the electrode. The depleted fuel and air from the fuel cell stack is then fed into a burner to produce heat from the unreacted methane, hydrogen and carbon monoxide. The exhaust from the burner is then sent to the fuel and air heat exchanger consecutively as described earlier. The exhaust gas from the air heat exchanger is then sent for heat recovery in the form of steam and hot water. The following sections provide a brief description and thermal model of different components of the fuel cell system.

Once the system model has been developed, it can be used to design model-based controller. The designing of the controller is dependent on the control objective and thus the key manipulated and controlled variables can also differ. For example, if the control objective is to improve load following performance of the system, then the stack voltage can work as a controlled variable whereas the fuel, steam and air (or, oxygen) flow rate to the fuel cell and the burner acts as manipulated variables for the controller. The flow rates can be controlled by using appropriate compressors, blowers and valves which can also be mathematically represented by ODE models. For this particular case, the split ratio of the exhaust gas to the heat recovery unit and heat exchangers can also act as a manipulated variable. The load and flow temperatures act as disturbances for the system. The detailed design of the controllers is however out of scope of this paper and thus is not discussed herein.

7.1. Fuel and air heat exchangers

Two heat exchangers have been used for preheating fuel and air in the fuel cell system. Both heat exchangers are assumed to be counter-current double pipe heat exchangers. A portion of hot stream which is the exhaust gas from burner is fed into the outer pipe and the cold stream is fed into the inner tube counter-currently. Assuming that the heat exchanger operates at constant pressure (a mild assumption), the general thermal model of the heat exchanger can be expressed as follows:

$$\rho C_p A \frac{\partial T}{\partial t} = -\rho C_p v A \frac{\partial T}{\partial z} + \pi D Q \tag{48}$$

where ρ is the gas density, C_p the heat capacity of the gas at constant pressure, A the cross-sectional area and Q is the heat transfer rate per unit area based on the heat transfer area πD.

Since the heat exchanger model as expressed in Eq. (48) is a partial differential equation, it is not a control relevant model. The model is thus converted into a set of ordinary differential equations by dividing the heat exchanger into n nodes along the flow direction as shown in Fig. 4. It is assumed that each node acts as a continuous stirred tank heater so that the temperature inside each node is same as the exit temperature of the gas of that particular node. Then energy balance of ith node for the tube (cold gas) and shell (hot gas) can be written as,

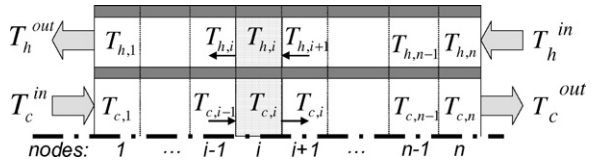

Fig. 4. Heat exchanger divided into n nodes along the length.

Table 1
Model parameters

Parameter	Value	Unit
Number of cells, N_0	384	
Cell area, A_c	100	cm^2
K_{H_2}	8.43×10^{-4}	kmol atm^{-1} s^{-1}
K_{H_2O}	2.81×10^{-4}	kmol atm^{-1} s^{-1}
K_{O_2}	2.52×10^{-3}	kmol atm^{-1} s^{-1}
$\tau^*_{H_2}$	26.1	s
$\tau^*_{H_2O}$	78.3	s
$\tau^*_{O_2}$	2.91	s
T^*	1000	°C
Constant resistance, r_0	0.126	Ω
Resistance slope, α	−2870	
Electrode thickness, h_e	0.25	mm
Interconnector thickness, h_i	1.5	mm
Electrode density, ρ_e	6.6	g cm^{-3}
Interconnector density, ρ_i	6.11	g cm^{-3}
Specific heat, $\bar{C}_{pe}$, $\bar{C}_{pi}$, $\bar{C}_{ps}$	0.4	J g^{-1} K^{-1}
Heat of reaction, $\Delta\hat{H}_r^\circ$	-0.2418×10^9	J $kmol^{-1}$
Emissivity, ϵ_a, ϵ_c, ϵ_i	0.9	

Table 2
Balance of plant parameters

Air heat exchanger:
$D_{i,tube} = 0.20$ m, $D_{o,tube} = 0.205$ m, $D_{i,shell} = 0.40$ m, $L = 10$ m
Fuel heat exchanger:
$D_{i,tube} = 0.05$ m, $D_{o,tube} = 0.055$ m, $D_{i,shell} = 0.10$ m, $L = 200$ m
Reformer:
Reaction area, $A_{RX} = 1000\,m^2$, reformer volume, $V_R = 10\,m^3$
Burner:
Burner volume, $V_B = 1\,m^3$

Tube:

$$\rho_c C_{pc} A_{cx} \frac{dT_c(i)}{dt} = -\rho_c C_{pc} v_c A_{cx} \frac{T_c(i) - T_c(i-1)}{\Delta z} + \pi D_0 U_0 (T_h(i) - T_c(i)) \quad (49)$$

Shell:

$$\rho_h C_{ph} A_{hx} \frac{dT_h(i)}{dt} = -\rho_h C_{ph} v_h A_{hx} \frac{T_h(i+1) - T_h(i)}{\Delta z} - \pi D_0 U_0 (T_h(i) - T_c(i)) \quad (50)$$

Here, subscripts 'c' and 'h' stand for the cold side and hot side energy balance; A_{cx} and A_{hx} for the cold and hot side flow cross-sectional area; Δz the length of each node; D_0 the outer diameter of the tube; and U_0[1] is the overall heat transfer coefficient based on D_0. The total number of ordinary differential equations for the lumped heat exchanger model in this case is $2n$.

[1] $U_0 = \left(\frac{r_0}{r_i h_i} + \frac{r_0 \ln(r_0/r_i)}{k_w} + \frac{1}{h_i}\right)^{-1}$.

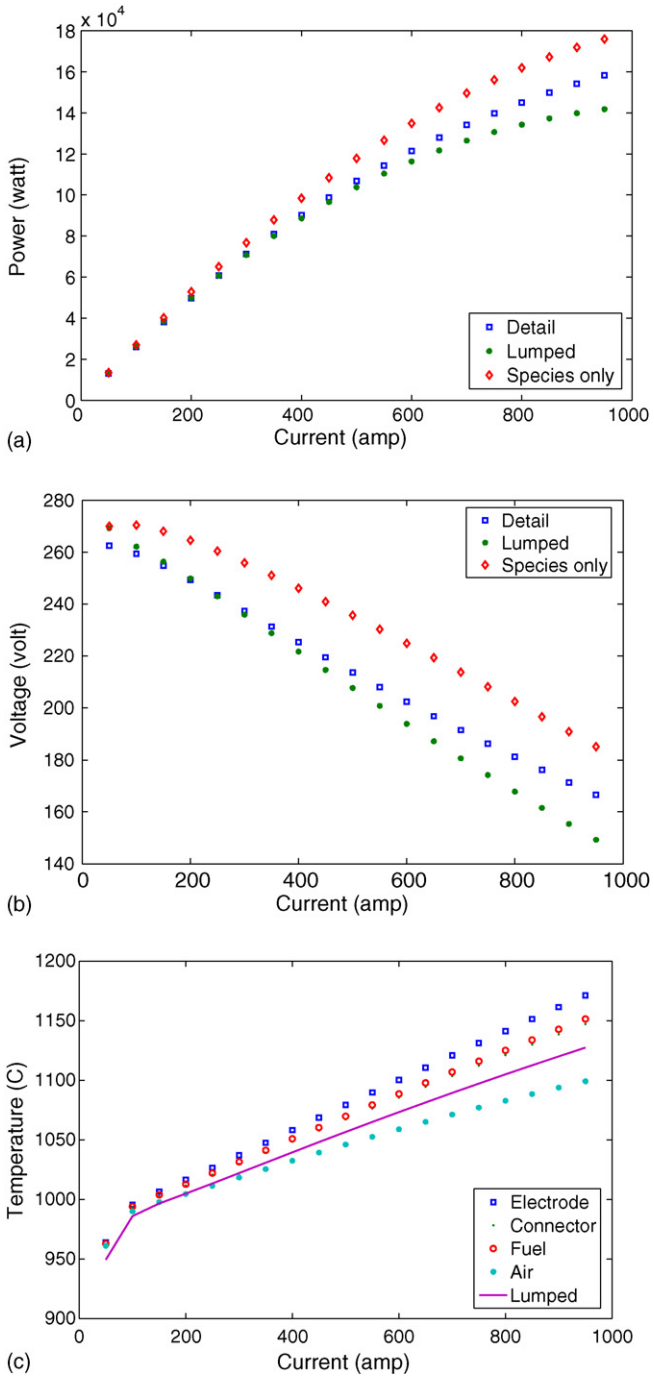

Fig. 5. (a) Power–current, (b) voltage–current and (c) temperature–current steady-state curves for planer SOFC.

7.2. Reformer

Preheated methane from the fuel heat exchanger and a separate stream of steam are fed into the reformer where endothermic reaction takes place between CH_4 and H_2O.

Reforming reaction:

$$CH_4 + H_2O \rightarrow CO + 3H_2, \quad \Delta\hat{H}_R^\circ = 206.1\,kJ\,mol^{-1} \quad (51)$$

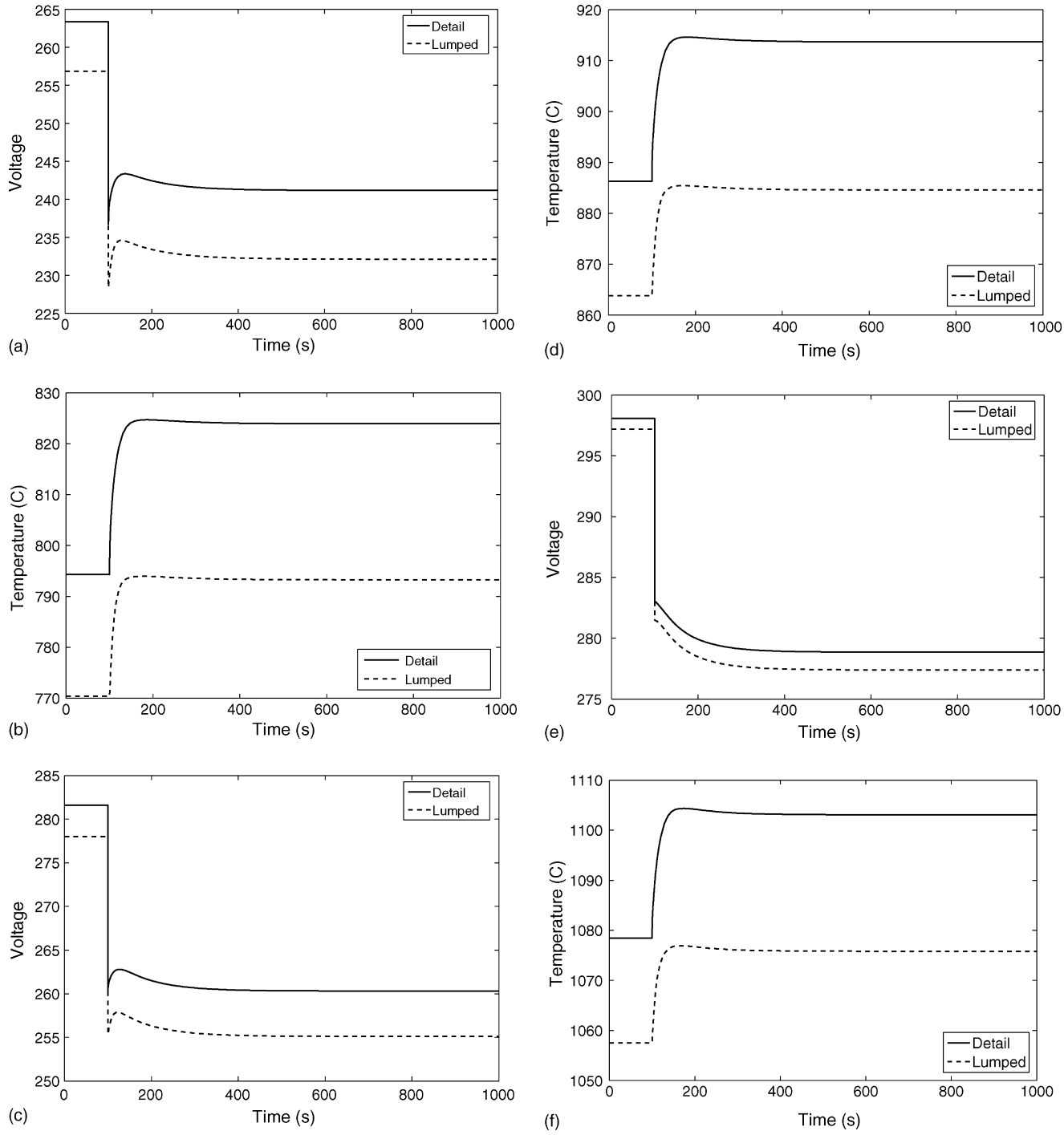

Fig. 6. Transient responses of voltage, power and temperature due to a load change of 500–600 A. Here, $\dot{n}_{H_2} = 5\,\text{mol}\,\text{s}^{-1}$; $\dot{n}_{O_2} = 10\,\text{mol}\,\text{s}^{-1}$; $T_{\text{fuel}}^{\text{in}}$ and $T_{\text{air}}^{\text{in}}$ are 700, 800 and 1000 °C for (a and b), (c and d) and (e and f), respectively.

If the reforming reaction rate is expressed by $\dot{r}_R$, then material balance for the reactant and product components are,

$$\dot{n}_{CH_4}^{\text{out}} = \dot{n}_{CH_4}^{\text{in}} - \dot{r}_R \tag{52}$$

$$\dot{n}_{H_2O} = \dot{n}_{H_2O}^{\text{in}} - \dot{r}_R \tag{53}$$

$$\dot{n}_{CO} = \dot{r}_R \tag{54}$$

$$\dot{n}_{H_2} = 3\dot{r}_R \tag{55}$$

where

$$\dot{r}_R = k_0 P_{CH_4} \exp\left(-\frac{E_A}{RT_R}\right) A_{RX}\,\text{mol}\,\text{s}^{-1} \tag{56}$$

$$k_0 = 4274\,\text{mol}\,\text{m}^{-2}\,\text{s}^{-1}\,\text{bar}^{-1} \tag{57}$$

$$E_A = 82\,\text{kJ}\,\text{mol}^{-1} \tag{58}$$

The mixture of CO and H_2O then take part in the reversible exothermic shift reaction to produce more hydrogen.

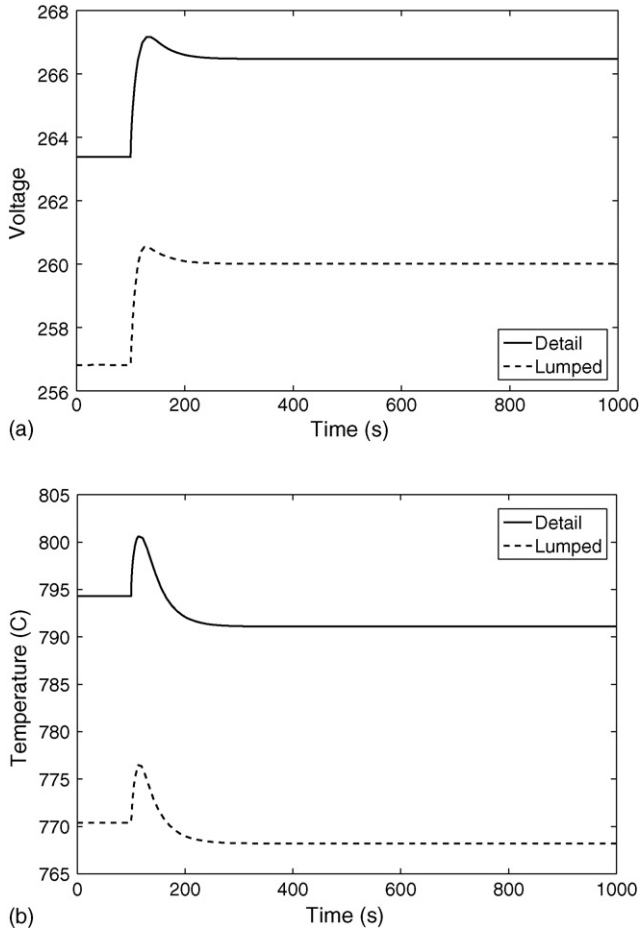

Fig. 7. Transient responses of voltage and temperature due to a change in hydrogen flow rate from 5 to 6 mol s^{-1}. Here, $\dot{n}_{O_2} = 10\,\text{mol s}^{-1}$; T^{in}_{fuel} and T^{in}_{air} are 700 °C.

Water–gas shift reaction:

$$CO + H_2O \rightleftharpoons CO_2 + H_2, \quad \Delta\hat{H}_S^\circ = -41.15\,\text{kJ mol}^{-1} \tag{59}$$

If the extent of reaction and equilibrium constant for the above reaction are expressed by ξ and K_S, respectively, then the material balance for the reactant and product components are,

$$\dot{n}^{out}_{H_2} = \dot{n}_{H_2} + \xi \tag{60}$$

$$\dot{n}^{out}_{CO_2} = \xi \tag{61}$$

$$\dot{n}^{out}_{CO} = \dot{n}_{CO} - \xi \tag{62}$$

$$\dot{n}^{out}_{H_2O} = \dot{n}_{H_2O} - \xi \tag{63}$$

where

$$K_S(T_R) = \frac{\xi(\dot{n}_{H_2} + \xi)}{(\dot{n}_{CO} - \xi)(\dot{n}_{H_2O} - \xi)} \tag{64}$$

The equilibrium constant K_S can be expressed as a function of temperature [4],

$$K_S(T_R) = \exp\left(\frac{5693.5}{T_R} + 1.077\ln T_R + 5.44\times10^{-4}T_R - 1.125\times10^{-7}T_R^2 - \frac{49,170}{T_R^2} - 13.148\right) \tag{65}$$

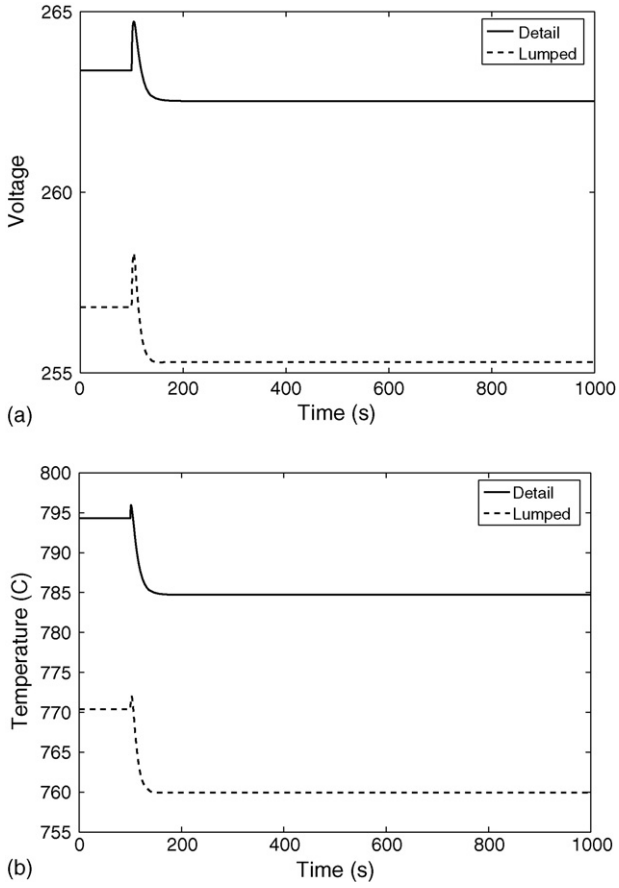

Fig. 8. Transient responses of voltage and temperature due to a oxygen flow rate change of 10 to 12 mol s^{-1}. Here, $\dot{n}_{H_2} = 5\,\text{mol s}^{-1}$; T^{in}_{fuel} and T^{in}_{air} are 700 °C.

Now that K_S is known, the extent of reaction can be calculated by solving Eq. (64). The energy balance around the reformer can then be written as,

$$\rho V_R C_p \frac{dT_R}{dt} = \dot{n}^{in}_{CH_4}\int_{T_{ref}}^{T^{in}_{CH_4}} C_{p,CH_4}(T)\,dT + \dot{n}^{in}_{H_2O}\int_{T_{ref}}^{T^{in}_{H_2O}} C_{p,H_2O}(T)\,dT - \sum \dot{n}^{out}_i \int_{T_{ref}}^{T_R} C_{p,i}(T)\,dT + r_R\Delta\hat{H}_R^\circ + \xi\,\Delta\hat{H}_S^\circ \tag{66}$$

where T_R is the reformer operating temperature.

7.3. Burner

The unreacted fuel and air from the fuel cell is then combusted together for heat recovery. In this stage it is important to supply additional oxygen so that all the unreacted fuel from fuel cell can be consumed. This is done by directly feeding the burner with another air stream. This also gives an additional degree of freedom for the controller to maintain system temperature within operating range. The underlying assumptions for building the burner model is given below:

- Enough O_2 is supplied so that all depleted gas from the fuel cell can be consumed.

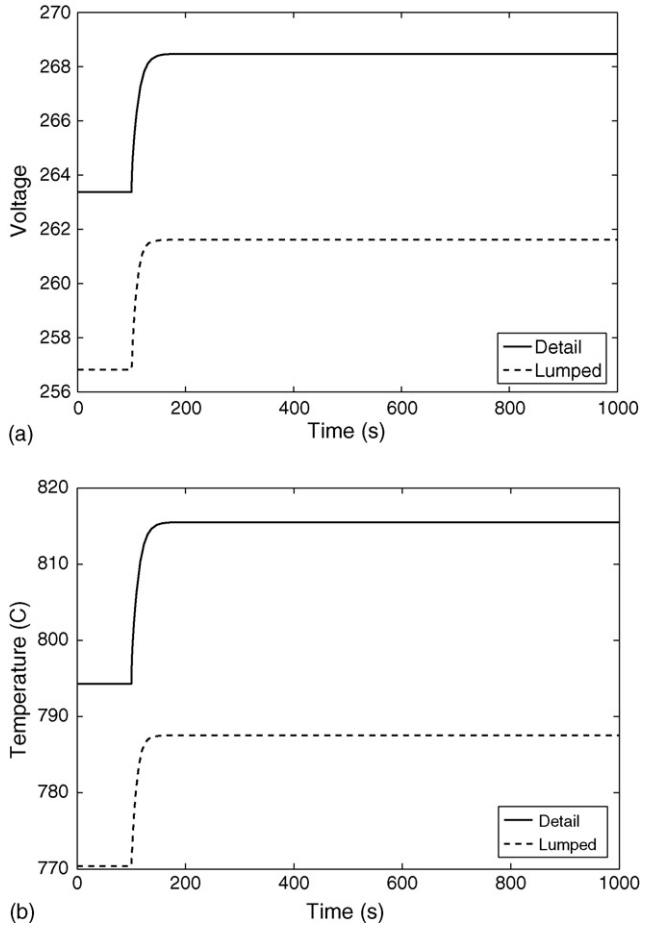

Fig. 9. Transient responses of voltage and temperature due to temperature change of fuel from 700 to 900 °C. Here, $\dot{n}_{H_2} = 5\,\text{mol}\,\text{s}^{-1}$; $\dot{n}_{O_2} = 10\,\text{mol}\,\text{s}^{-1}$; current load is 500 A; and $T^{\text{in}}_{\text{air}}$ is kept constant at 700 °C.

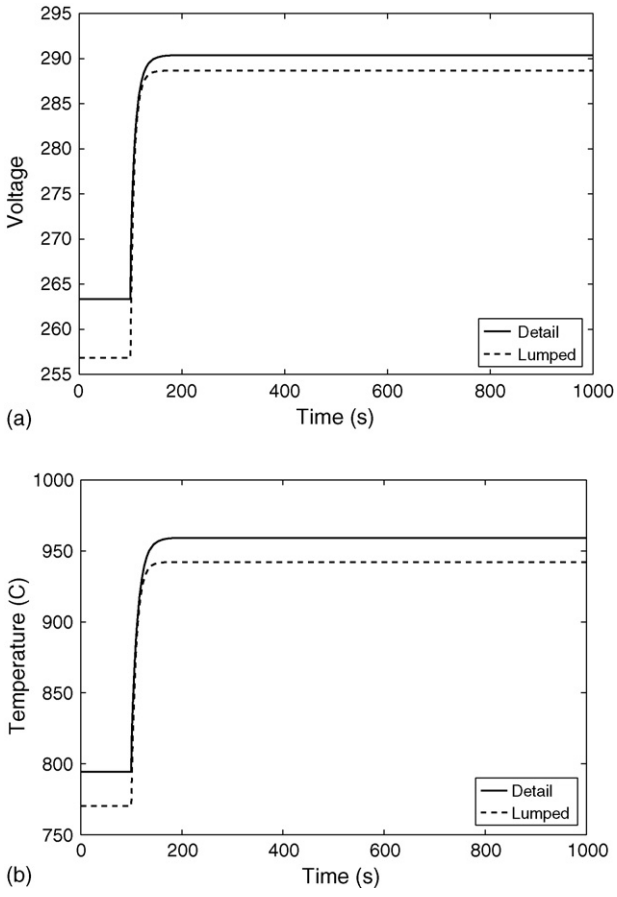

Fig. 10. Transient responses of voltage, power and temperature due to temperature change of air from 700 to 900 °C. Here, $\dot{n}_{H_2} = 5\,\text{mol}\,\text{s}^{-1}$; $\dot{n}_{O_2} = 10\,\text{mol}\,\text{s}^{-1}$; current load is 500 A; and $T^{\text{in}}_{\text{fuel}}$ is kept constant at 700 °C.

- Ideal gas mixing inside the burner chamber so that the exit temperature of the burner is same as the inside temperature.
- Burner operates at constant pressure.

Energy balance around the burner,

$$\rho V_{\text{B}} \bar{C}_p \frac{\text{d}T_{\text{B}}}{\text{d}t} = \sum \dot{n}^{\text{in}}_{i\text{F}} \int_{T_{\text{ref}}}^{T_{\text{F}}} C_{p,i}(T)\,\text{d}T + \sum \dot{n}^{\text{in}}_{i\text{A}} \int_{T_{\text{ref}}}^{T_{\text{A}}} C_{p,i}(T)\,\text{d}T - \sum \dot{n}^{\text{out}}_{i\text{B}} \int_{T_{\text{ref}}}^{T_{\text{B}}} C_{p,i}(T)\,\text{d}T - \dot{n}^{\text{in}}_{\text{H}_2} \Delta \hat{H}_{\text{r,H}_2}{}^{\circ} - \dot{n}^{\text{in}}_{\text{CH}_4} \Delta \hat{H}_{\text{r,CH}_4}{}^{\circ} - \dot{n}^{\text{in}}_{\text{CO}} \Delta \hat{H}_{\text{r,CO}}{}^{\circ} \quad (67)$$

where T_{B} is the burner temperature; subscripts 'F', 'A' and 'B' stand for fuel, air and burner, respectively; the specific heat $\bar{C}_p$ and the density ρ are also calculated empirically at each computational instance.

8. Simulation result

The lumped and detailed models deduced in Sections 4 and 5 can be used for simulating fuel cell behavior under different operating conditions. By considering reforming reaction kinetics, it can also be extended to include internal reforming and thus be used to simulate SOFC behavior with natural gas as fuel. Since these models comprise a set of nonlinear ODEs, they can also be used to design model-based controller.

The objective of this paper is to synthesize the SOFC cell model with that of BOPs to form a control relevant dynamic model in system level. The synthesis is by no means a simple assembly of the existing models. For example, in order for the system to be controllable, additional component with the associated differential equation is needed to avoid the sudden drop of voltage due to step change of load. In addition, to make the complex system model control relevant, many component models including the cell model have to be re-established. However, the model parameters needed to be populated from experimental and/or literature data for simulation and controller design. Most of these data are extracted from [19,21,5,23,20]. Some model parameters are not available and thus have been estimated empirically within sensible limits. The parameters of the balance of plant components can be estimated based on the capacity of the respective units using engineering design practice. In this work, the key parameters are estimated iteratively so that the operating conditions can be met at steady-state. Tables 1 and 2 contain the parameters of a planar SOFC stack made from 384 cells connected in series and the parameters of a SOFC system.

8.1. Fuel cell

The lumped and detailed models are used to generate power–current, voltage–current and temperature–current steady-state curves for a fixed 85% fuel utilization[2] and excess oxygen flow ratio of four times stoichiometric value. The inlet temperatures of fuel and air were kept constant at 700 °C. The simulations were done using MATLAB 7.0 by considering the ohmic loss in order to compare the results with species-only model described in [19]. The existing solvers in MATLAB however can not solve differential algebraic equation (DAE) of DAE index greater than 1. Thus, the exit temperatures of fuel and air gases in the detail model have been calculated using the ODEs [Eqs. (34) and (38)] instead of the algebraic equations expressed by Eqs. (37) and (41), respectively.

Fig. 5(a and b) shows the steady-state power and voltage output from the lumped, detail and species-only dynamic models. Here, the operating temperature of the species-only dynamic model [19] is assumed to be 900 °C. From the figures, it is evident that the power and voltage predictions from the proposed models are comparable whereas the species-only dynamic model predicts higher cell terminal power and voltage. In fact, the stack voltage and power predicted by the species-only model depends on the cell operating temperature which is dependent on the fuel and air inlet temperature as well as the demand current. Thus, instead of being constant, it varies with operating conditions and thus the assumption of constant fuel cell temperature is not valid.

The stack temperature from the lumped model and the temperatures of electrode, interconnector, depleted fuel and air gases are shown in Fig. 5(c). From the figure it is seen that with increase in current load fuel cell operating temperature increases. It is also to be noted that the difference in exit temperatures of fuel and air gases increases with increase in current load which are different from the uniform cell temperature of the lumped model. Since stack voltage is a function of the fuel cell temperature, the output stack voltage from the fuel cell described by the lumped and detail model also differs at higher demand current as shown in Fig. 5(b).

Simulations were also conducted to compare the transient responses of the fuel cell described by the lumped and detail models. The transient response of the fuel cell in terms of fuel cell stack voltage and cell temperature has been investigated by changing the current loads, fuel and air flow rates as well as their inlet temperatures (Figs. 6–10). The transient response of fuel cell stack voltage and cell temperature expressed by the models due to an increase in current load from 500 to 600 A is shown in Fig. 6. Here fuel and O_2 flow rates are kept constant at 5 and 10 mol s^{-1}, respectively. The inlet temperatures of fuel and air however are 700 °C for Fig. 6(a and b), 800 °C for Fig. 6(c and d) and 1000 °C for Fig. 6(e and f).

From the simulation results, it is noticed that the dynamic behavior of the fuel cell stack voltage is greatly dependent on the inlet temperatures of fuel and air entering the fuel cell. For

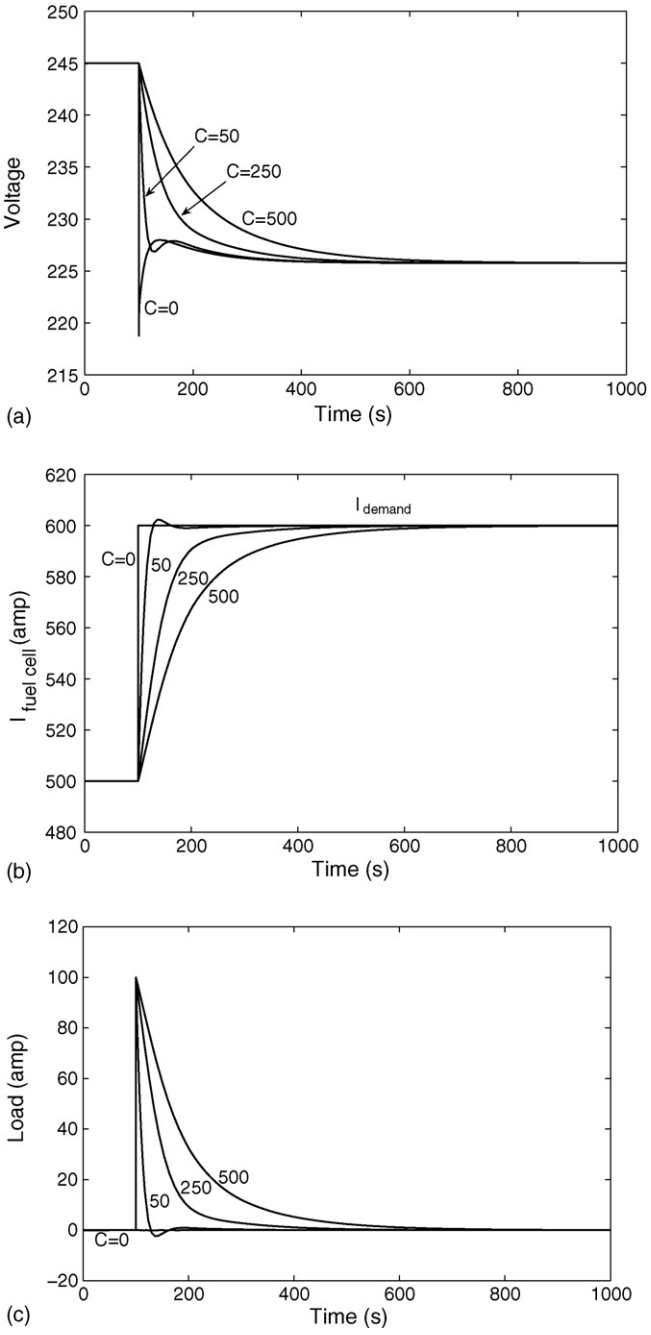

Fig. 11. (a) Voltage response of SOFC connected in parallel with a capacitor. Demand current sharing by (b) the fuel cell and (c) the capacitor.

all the cases, there is a sudden drop in the voltage associated with the step increase in the load. This sudden voltage drop comes from the ohmic loss term $r(T)I$ in the expression of stack voltage Eq. (14). However, since the fuel cell stack temperature, T_s, in the lumped model and electrode temperature, T_e, in the detailed model are function of the current load, they also increase with an increase in the load (Fig. 6(b, d and f)). The increase in the cell temperature is associated with a decrease of both internal resistance, $r(T)$ in the ohmic loss term and the standard electrode potential, ΔE_0 as shown in Eqs. (18) and (16), respectively. Thus, there is a net gain or loss in the stack voltage depending on the magnitude of ohmic loss and standard electrode potential.

[2] Fuel utilization, $U_f = \frac{\dot{n}^r_{H_2}}{\dot{n}^{in}_{H_2}}$.

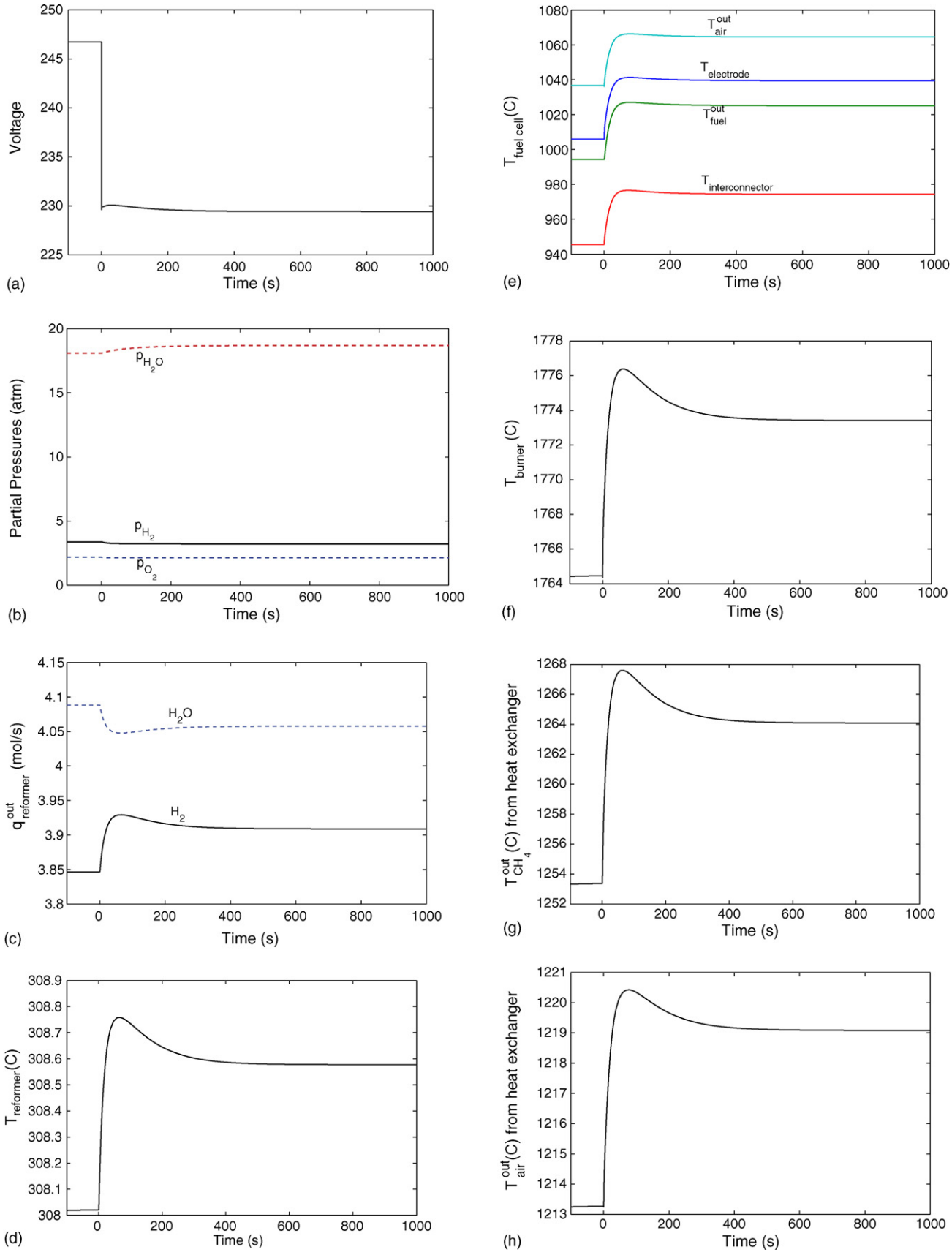

Fig. 12. Transient responses of fuel cell system due to load change from 500 to 550 A. Here, $\dot{n}_{CH_4} = 3\,\mathrm{mol\,s^{-1}}$; $\dot{n}_{O_2} = 6\ \mathrm{mol\,s^{-1}}$; $\dot{n}_{H_2O} = 6\,\mathrm{mol\,s^{-1}}$; $\dot{n}_{O_2,\mathrm{burner}} = 10\,\mathrm{mol\,s^{-1}}$; inlet temperature of the fuel and air are 25 °C and $T_{H_2O} = 150\,^{\circ}\mathrm{C}$.

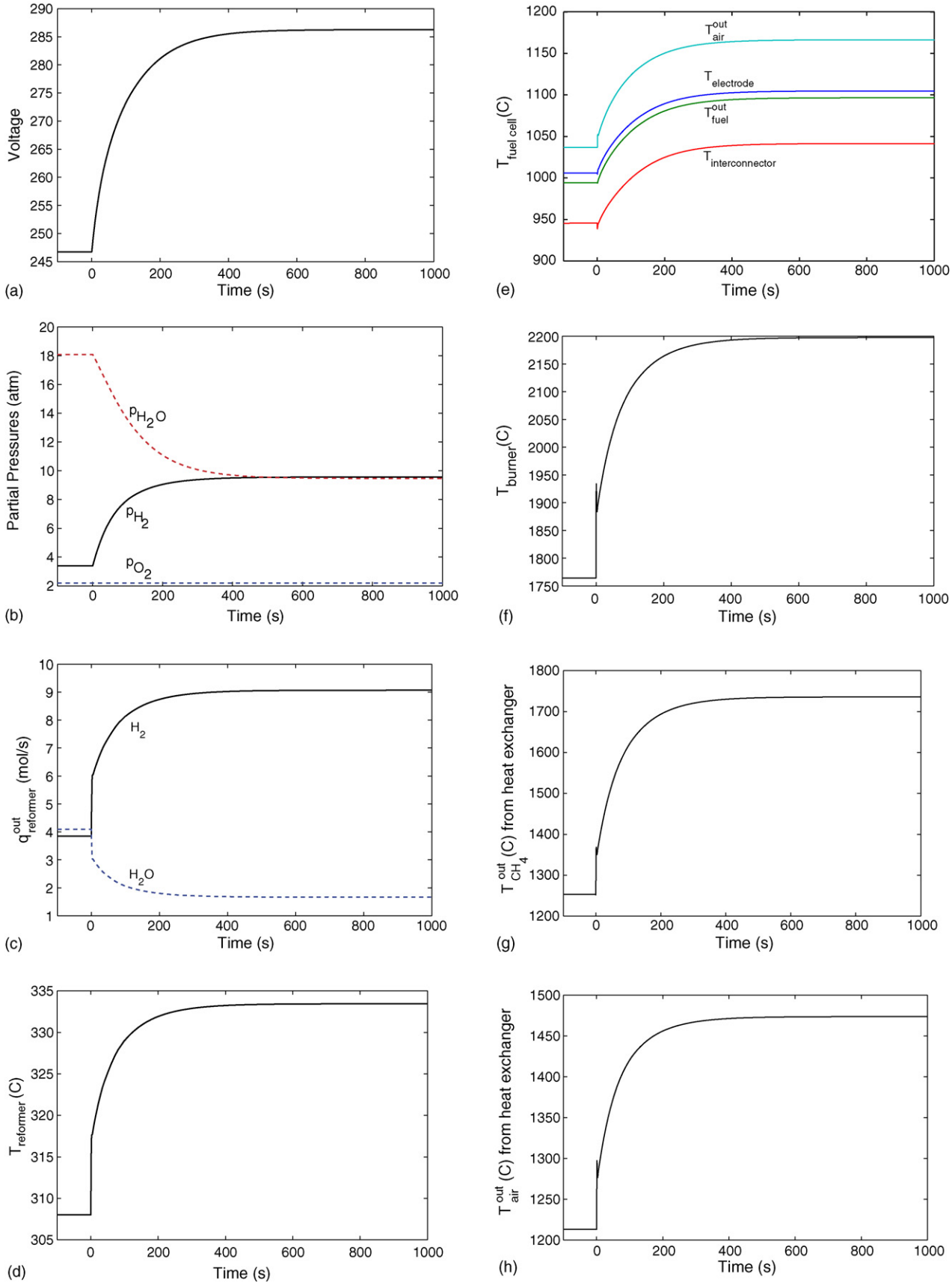

Fig. 13. Transient responses of fuel cell system due to change in methane flow rate from 3 to 4 mol s^{-1}. Here, current load $I = 500$ A; $\dot{n}_{O_2} = 6$ mol s^{-1}; $\dot{n}_{H_2O} = 6$ mol s^{-1}; $\dot{n}_{O_2,burner} = 10$ mol s^{-1}; inlet temperature of the fuel and air are 25 °C and $T_{H_2O} = 150$ °C.

For low fuel and air inlet temperatures (700 °C), there is a net gain of stack voltage from the initial drop (Fig. 6(a)). However, as the inlet temperatures of fuel and air are increased, the gain of voltage due to decrease in the ohmic resistance is overshadowed by the decrease in the standard electrode potential. This behavior results in the gradual decreasing of the stack voltage from the initial voltage drop as shown in Fig. 6(c and e).

The transient behavior of the fuel cell in terms of voltage and cell temperature for a step change in the fuel flow rate, $\dot{n}_{H_2}$, from 5 to 6 mol s^{-1} is shown in Fig. 7. The current load I, O_2 flow rate $\dot{n}_{O_2}$ and the inlet temperature of fuel and air are kept constant at 500 A, 10 mol s^{-1} and 700 °C, respectively. Figs. 8–10 show the transient responses for a step change in O_2 flow rate from 10 to 12 mol s^{-1}, and step changes in the inlet temperature of fuel and air from 700 to 900 °C, respectively.

8.2. Fuel cell with capacitor

For a stand-alone SOFC, the voltage drops suddenly when the load was increased from 500 to 600 A [see Fig. 7]. However, when the fuel cell is connected in parallel with a capacitor, the combined system behaves as a first-order system. As the capacitance of the capacitor is increased from 0 to 500 F for the combined system, the load sharing capability of the capacitor increases [Fig. 11(b and c)] and the sharp decline in the voltage is smoothed out [Fig. 11(a)]. In other words the capacitor works like a filter for the demand current. The final steady-state stack voltage for all the cases are same which is evident from Eq. (47).

8.3. Fuel cell system simulation

The fuel cell system described in the previous section is simulated for a demand current change of 500–600 A keeping all other input flow rates and disturbances constant. The balance of plant parameters, used in the simulation, are designed so that operating constraints are met and are presented in Table 2. The dynamic response of the fuel cell system in terms of stack voltage and different component temperatures is shown in Fig. 12. Since the stack voltage of the fuel cell system is dependent on the input flow rates and temperatures, the prediction of voltage is not straightforward. For example, for this case increase in demand current is associated with increase in the fuel and air inlet temperature of the fuel cell as well as increase in hydrogen production rate and decrease in steam out of the reformer. But since partial pressures are not only a function of the corresponding flow rates, but function of temperatures as well, the partial pressures of H_2 and H_2O decreased and increased, respectively, resulting in additional loss in the stack voltage.

For an increase in the methane flow rate, the stack voltage from the fuel cell system increases due to increase and decrease in the hydrogen and steam partial pressures, respectively, as shown in Fig. 13. Here, the hydrogen production from reformer increases as well as the reformer temperature, fuel cell inlet flow temperatures and burner exhaust temperature. The increase in hydrogen flow rate increases the partial pressure which finally results in the increase of stack voltage.

9. Conclusion

The main objective of this work was to develop control relevant model of the fuel cell system so that it can be used to design model-based controller. For this purpose, two sets of comparable models, lumped and detail model both represented by zero-dimensional nonlinear ODEs, have been developed. Simplified thermal models of system components have also been provided. The advantage of using capacitor in parallel with the fuel cell is discussed with appropriate formulation and simulations. Simulations are conducted for both of the models and entire system to compare steady-state and dynamic behavior. From the simulations as well as the understanding of the model, the following conclusions can be drawn:

- SOFC temperature is an important variable in predicting stack voltage and thus species-only model which assumes constant operating temperature is not valid unless an isothermal operation is enforced by other heating device.
- Stack voltage, current load and cell temperature are internally dependent. Change of one affects all of the others. This is more prominent in the fuel cell system with after-burner and heat exchangers. Change in fuel flow rate or demand current or even inlet temperature leads to a change in hydrogen flow rate in the fuel cell from the reformer. This leads to a change in fuel cell temperature and stack voltage. The unreacted fuel then goes to after-burner and heat exchangers which again affects the temperatures of the reformer and fuel cell. The effect of flow rates or disturbances thus propagates through the entire fuel cell system.
- Steady-state stack voltage, power and temperature of the fuel cell predicted by both of the models are comparable at lower current load. But as the current load is increased they differ in magnitude and thus it is important to choose appropriate model depending on the control objective. For example, for designing a controller where computational power is limited, the lumped model can be used. But for evaluating performance of the fuel cell, detail model is preferable. In addition, the lumped model considers that the exit temperature of depleted fuel and air are same. In fact, these temperatures differ widely for higher current load and thus detail model should be used, especially when the fuel cell is connected to an after-burner for recovering energy.
- At lower operating temperature, the stack voltage initially drops suddenly for a step up of the current load and then gains some voltage due to decrease in ohmic loss. But at higher operating temperature, the gain in stack voltage due to lower ohmic loss is overshadowed by the decrease in standard electrode potential resulting in more decrease in the stack voltage from the initial drop. Thus, fuel cell may show different dynamic characteristics depending on the operating region.
- For the detail model exit temperatures of fuel and air can be expressed either by ODEs or by DAEs. However, solving DAE may require additional computational power and may not be helpful if the model is used to compute future control actions using optimization algorithms such as MPC. Thus,

in our simulation ODEs have been used to simulation exit temperature of fuel and air out of fuel cell.

- Capacitor can act as an auxiliary power source for the fuel cell system soothing out sudden change in the voltage. It can help in two ways: first, electrical equipments will be less prone to damage due to the sudden fluctuation in the voltage, and second, any controller responsible for maintaining the voltage will be able to bring the voltage to its reference value more easily.
- It is to be noticed that the lumped and detail models are described by nonlinear ODEs with 4 and 7 states, respectively. Hence, during simulation the performance of lumped and detail models do not differ much in terms of computational time. For example, the cpu time to simulate the transient response for load change described by lumped and detail models are 0.6409 and 0.8012 s, respectively [Fig. 6(a and b)]. The computation, in this particular case, is performed using Dell Inspiron 600 M with 2.00 GHz Intel Pentium Mobile processor and 1 GB RAM running Microsoft Windows XP Home as an operating system. For control purpose, which is not presented in this paper, the cpu time for linear controller (e.g., linear MPC) does not differ much. But for nonlinear controller obviously the computational time is higher based on the sample time to estimate unmeasured states using nonlinear state estimator (e.g., unscented Kalman filter) and the sample time of the controller (e.g., nonlinear MPC). However, with the advent of cheap computational power and dedicated servers for applying advanced controller, this is not a problem anymore.

Overall, the developed models can predict all the important variables of the fuel cell system. In addition the models being zero-dimensional in nature can be used for designing model-based controller such as linear and nonlinear MPC. Moreover since usually all the states are not measurable, the same model can be used for estimating states using state estimator such as extended Kalman filter (EKF) or, unscented Kalman filter (UKF).

References

[1] E. Achenbach, J. Power Sources 57 (1995) 105–109.
[2] N.F. Besset, W.J. Wepfer, J. Winnick, J. Electrochem Soc. 142 (11) (1995) 3792–3800.
[3] R. Bove, P. Lunghi, N.M. Sammes, Int. J. Hydrogen Energy 30 (2005) 181–187.
[4] R. Bove, P. Lunghi, N.M. Sammes, Int. J. Hydrogen Energy 30 (2005) 189–200.
[5] R.J. Braun, Optimal design and operation of solid oxide fuel cell systems for small-scale stationary applications, Ph.D. Thesis, University of Wisconsin-Madison, 2002.
[6] S.H. Chan, O.L. Ding, Int. J. Hydrogen Energy 30 (1) (2005) 167–179.
[7] S.H. Chan, H.K. Ho, O.L. Ding, Fuel Cells 5 (1) (2005) 25–33.
[8] D.L. Damm, A.G. Fedorov, J. Power Sources 143 (2005) 158–165.
[9] R.M. Felder, R.W. Rousseau, Elementary Principles of Chemical Processes, second ed., John Wiley & Sons, Inc., 1986.
[10] D.J. Hall, R.G. Colclaser, IEEE Trans. Energy Conver. 14 (3) (1999) 749–753.
[11] E. Hernandez-Pacheco, M.D. Mann, P.N. Hutton, D. Singh, K.E. Martin, Int. J. Hydrogen Energy 30 (2005) 1221–1233.
[12] P. Iora, P. Aguiar, C.S. Adjiman, N.P. Brandon, Chem. Eng. Sci. 60 (3) (2005) 2963–2975.
[13] H.-J. Jahn, W. Schroer, Fuel Cells 4 (4) (2004) 276–282.
[14] J. Larminie, A. Dicks, Fuel Cell Systems Explained, second ed., John Wiley & Sons, Ltd., 2003.
[15] R.T. Leah, N.P. Brandon, P. Aguiar, J. Power Sources 45 (2005) 336–352.
[16] J.H. Lienhard IV, J.H. Lienhard V, A Heat Transfer Textbook, third ed., Phlogiston Press, Cambridge, MA, 2005.
[17] L. Magistri, A. Traverso, F. Cerutti, M. Bozzolo, P. Costamagna, Fuel Cells 5 (1) (2005) 80–96.
[18] P. Aguiar, C.S. Adjiman, N.P. Brandon, J. Power Sources 147 (2005) 136–147.
[19] J. Padulles, G.W. Ault, J.R. McDonanld, J. Power Sources 86 (2000) 495–500.
[20] R.H. Perry, D.W. Green J.O. Maloney (Eds.), Perry's Chemical Engineers' Handbook, seventh ed., McGraw Hill, USA, 1997.
[21] K. Sedghisigarchi, A. Feliachi, IEEE Trans. Energy Conver. 19 (2) (2004) 423–428.
[22] A. Selimovic, M. Kemm, T. Torisson, M. Assadi, J. Power Sources 145 (2005) 463–469.
[23] EG&G Technical Services and Science Applications International Corporation, Fuel Cell Handbook, sixth ed., US Department of Energy, 2002.
[24] C. Stiller, B. Thorud, O. Bolland, R. Kandepu, L. Imsland, J. Power Sources 158 (1) (2006) 303–315.